Measurement and Simulation of DI Spray Impingements and Film Characteristics

Yi Zheng[1*], Xingbin Xie, Ming-Chia Lai
Wayne State University, USA
dz7403@wayne.edu

Brad VanDerWege
Ford Motor Co., USA
bvanderw@ford.com

Abstract

Spray impingement of liquid fuel on the combustion chamber wall and piston head in the direct injection engine is difficult to avoid and mostly undesirable, because it delays the gas-phase fuel-air mixture preparation processes and is a possible source for unburned hydrocarbons and soot emissions. This work investigated wall impingement and surface fuel film formation by sprays emerging from a side-mounted six-hole gasoline injector, one of the most dominant direct injection (DI) gasoline engine combustion configuration used today. The fuel was injected on the ground glass diffuser window surface at various ambient conditions in a pressurized chamber using the same optical setup. Different air pressure and temperature, injection pressure and duration, and distance between the injector tip and window were investigated. The spray wetted area, fuel film thickness, and the resultant footprint mass were derived using the Refractive Index Matching (RIM) technique. As expected, the deposit area of each spray plume is affected by the injection pressure and distance between injector tip and window. The effect of ambient temperature on fuel film thickness is significant, so is the ambient pressure on the film evaporation rate, especially at lower temperature. Multi-dimensional computational fluid dynamics (CFD) simulation with selected models of spray validated first for its transport in the air is used to compare the impingement models with the experimental measurements. The fuel film shapes were in very good agreement, however, the thickness and mass history was only in fair agreement, possibly due to limitations of the experimental techniques and the model accuracy.

Introduction

Spray impingement on solid surface occurs in many industrial and technical processes [1]. Recent surge in Direct Injection (DI) gasoline engine in passenger vehicle sale demonstrates the success in reducing both pollutant emissions and fuel consumption. However, the impingement of liquid fuel on the combustion chamber wall and piston head in the direct injection engine is mostly undesirable although difficult to avoid, because it affects mixture preparation prior to combustion and is a possible source for unburned hydrocarbon (UHC) and particulate matter emissions [2], which is the focus of future particle-number-based emission standards. The problem of wall impingement has been studied quite extensively experimentally and computationally for DI diesel, port-injection and DI gasoline [3-12]. For gasoline-fueled engines, port fuel injection generally produces a thicker fuel film than DI because of the lower injection pressure and ambient temperature compared to DI cases. It has also been suggested that the level of soot emissions is more strongly dependent on the wall film thickness than the total amount of fuel on the piston head [13]. The fuel film formed on the piston head in direct-injection engines was measured quantitatively by Refractive Index Matching technique (RIM) by Drake et al. [14], [15]. This relatively simple optical method can be used for quantitative temporal and spatial measurements of fuel film under vaporizing conditions. The results showed that the area-average film thickness is around 1μm and the maximum film is about 3μm [15], [16]. Liquid film formation and precise thickness measurement have also been analyzed by RIM measurements and qualitative LIF visualizations for direct injection SI engines [17] using piezo outward opening nozzles. The maximum peak film thicknesses is found to be in the range of 0.9-1.0μm, and that faster evaporation rates occur at the outer edges of the film with smaller thickness.

Multi-dimensional CFD offers a promising alternative to experiments for its capability to offer much more detailed information on mixture formation and spray impingement. Numerical methods are still a challenge today, mainly because the sub-models used to simulate the physical phenomena of injection spray and droplet impingement are not sufficiently validated. Thus there is a need for more accurate models and experimental parameters influencing the spray-wall interaction [18]. The spray droplets undergo a number of modeled processes including breakup, collision, vaporization and drop drag. If the fuel spray impacts the piston surface, then the formation and evaporation of liquid fuel films should be considered. Among these physical processes, the breakup process is the most sensitive to the prediction of droplet velocity and size. The current numerical study is conducted using Kelvin-Helmholtz/Rayleigh-Taylor (KH-RT) breakup model based on the competition between KH and RT instabilities, and has been to shown to have good agreement with experimental results in the

* Corresponding author: dz7403@wayne.edu

general spray shape, and the distributions of Sauter mean diameter (SMD) and velocity [19]. In other relevant study, the coupled Eulerian-Lagrangian method has been used to correlate the injector internal flow and near-field primary atomization [20] without the limitation of aerodynamic breakup. The wall film thickness for diesel spray impingement has been simulated by considering and evaluating the heat transfer between the temperature-controlled wall and impinging spray [21]. The effects of injection pressure and wall inclination angle on the macroscopic behavior of a multi-hole GDI spray were investigate experimentally and numerically [22]. The behavior of the spray impingement was observed using a optical access engine, however the amount of liquid film remaining on the piston crown appears under-predicted after compared with simulation results [23].

In this work, the formation and evolution of the fuel spray emerging from a side-mounted six-hole injector in a pressurized chamber were investigated by spray visualization, and the fuel film thickness on the ground diffuser ground glass was measured using RIM techniques. In the meanwhile, numerical study was conducted for the same operating conditions as the experiments to study the spray behavior and fuel film characteristics.

Experimental Setup

Experiment apparatus were setup to calibrate and measure the liquid fuel film thickness for multi-hole injectors using Refractive Index Matching technique. Figure 1 shows a schematic diagram of the experiment apparatus and optical setup for liquid fuel film calibration and measurement.

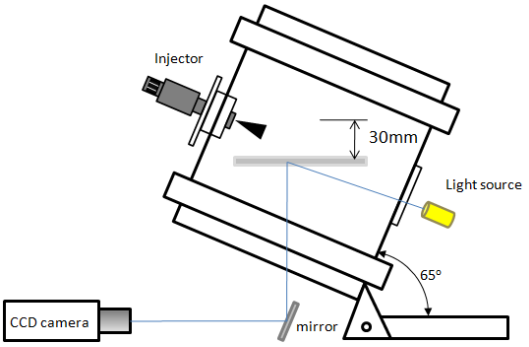

Figure 1 Experimental setup of RIM visualization.

The six-hole GDI injector was mounted on the cylinder wall of the chamber with angle of 25 deg. The injection specifications are shown in Table 1. Two 140mm diameter 50mm thick quartz windows were mounted on the sides of the inclined pressurized chamber (the inclination angle of the camber is 65 deg) and one 60mm diameter 20mm thick quartz window was on the bottom. The pressurized chamber can be heated up to 250°C by a circulation air heater and pressured up to 4bar. A flat optical ground glass diffuser (N-BK7, Thorlabs), 100mm × 100mm, 2mm thick was placed in the pressurized chamber horizontally. Various grit polishes on the diffuser were tested, but the results presented of this paper were obtained using the 220 grit polish, which shows the best sensitivity to the range of film thickness of interest, which is around 1 micron. Lighting was provided by a continuous projection lamp from the side window with an incident angle of about 10°. The images were captured with the high speed digital CCD camera through a mirror placed directly beneath the impingement surface and outside the spray chamber. A liquid mixture of a high volatility component (iso-octane) and a low volatility component (dodecane) with known deposit volume was used for calibration procedure similar to a recent study by Maligne and Bruneaux[17]. Spray impingement and liquid film thickness measurements were performed using iso-octane as fuel. The index of refraction of Iso-octane and dodecane is 1.40 and 1.42 respectively, which is close to the index of refraction of the window material, 1.46.

Table 1 Injector specifications and spray targeting

Number of holes	6
Nozzle diameter (mm)	0.228
Nozzle length (mm)	0.285
Averaged L/D ratio	1.25
Static mass flow with N-Heptane (g/s)	15.4

Table 2 shows the reference conditions for a direct injection engine. Multi-hole injector was mounted with 25 deg to simulate a side-mounted DI engine configuration. Iso-octane was used as reference fuel. Different chamber pressure and temperature, injection pressure and duration, and distance between the injector tip and window were investigated.

Table 2 Operating conditions

Case #	1	2	3	4	5	6	7	8	9	10
Distance	30	30	40	40	30	30	30	30	30	30
Air pressure (bar)	1	1	1	1	1	2	1	2	1	2
Air temperature (°C)	50	50	50	50	50	50	75	75	100	100
Injection pressure (bar)	35	140	35	140	70	70	70	70	70	70
Fuel temperature (°C)	40	40	40	40	40	40	55	55	70	70
Pulse width (ms)	2.83	1.41	2.83	1.41	2	2	2	2	2	2

Refractive Index Matching Method

The RIM technique measures the spatial distribution of the fuel film thickness, from which the adhered puddle mass can be calculated. In this method, the difference in index of refraction between the impinging surface and air results in the scattering of light off the roughened surface, which is modified by the presence of a liquid that closely match the index of refraction of the impingement window [16]. Drake *et al*. [14,15] showed that the relation between the fuel film thickness and the variation of intensity in the scattered light. The reflection variation (reduction) ΔI through the window was written as:

$$\Delta I(x,y) = 1 - \frac{I_{wet}(x,y)}{I_{ref}(x,y)} \tag{1}$$

where I_{ref} is the intensity of the scattered light in a reference image at location of (x,y) and I_{wet} is the intensity with the fuel deposit.

A calibration procedure was performed to obtain a function f for the fuel film thicknesses $h(x,y)$ and the reflection variation in the scattered light ΔI :

$$h(x,y) = f(\Delta I) \tag{2}$$

The calibration experiment was carried out at ambient condition to obtain the correlation between fuel film thickness and variation of reflection. The experiment setup is the same as shown in Figure 1, but without the injection system.

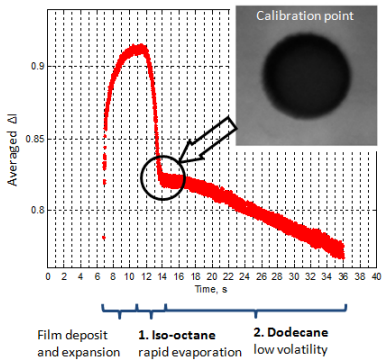

Figure 2 Evolution of averaged reduction ΔI on the window

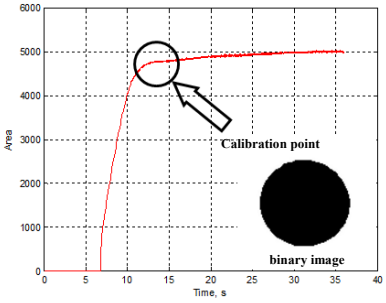

Figure 3 Evolution of deposit wetting area

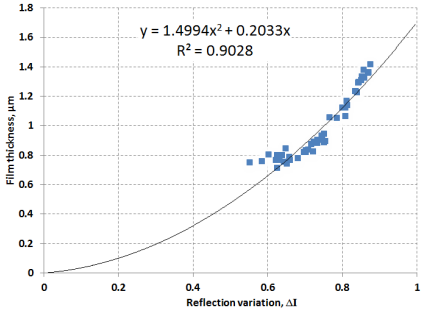

Figure 4 Calibration curve for the rough window between liquid film thickness and reduction, ΔI

A liquid mixture of 10% by volume of dodecane and 90% by volume of iso-octane was used for calibration procedure. Figure 2 and 3 shows the time evolution of the averaged reduction in the scattered light ΔI and deposit area. The liquid mixture was dripped on the dry window by syringe and the scattering reduction value increased from 0 to maximum. After the deposited film expanded, the mixture rapidly evaporated as noted in stage 1 in Figure 2. The corresponding reduction ΔI dropped in less than 3 second to the calibration point. It is assumed that the high volatility component (iso-octane) in the mixture was completely evaporated before this calibration point and only the low volatility component (dodecane) remained on the window surface [17]. The dodecane then evaporated relatively slowly and the scattering reduction ΔI decreased to the value of dry window in around 24 seconds after the calibration point.

At the calibration point, the dodecane volume and the corresponding deposit area, as shown in Figure 3, were used to obtain the fuel film thickness. The minimum volume delivered by the syringe was 0.1μL in this study. Therefore, the dodecane volume was calculated as 10% of the initial volume of mixture droplet, which provided a very thin film thickness. Figure 3 shows the film wetted area at calibration point. The threshold value of this deposit area in the binary image was found using Otsu's method in MATLAB software and the number of pixels below the threshold was counted to obtain the size of area. It is assumed that the film thickness is uniform. Therefore, the fuel film thickness could be obtained at the calibration point from the dodecane volume and the wetted area. The averaged reference dry image was obtained before the liquid was deposited on the window surface. The mean reduction in the scattered light ΔI can be calculated from Equation (1). The calibration technique used in the current system is not sensitive enough to resolve thickness below 0.5 microns, and thicknesses less than that are extrapolated to zero point by default. After repeating a range of liquid volumes, the calibration relation curve was found using Equation (2) as shown in Figure 4.

After the calibration procedure, the six-hole injector was mounted on the cylinder wall of the chamber with angle of 25 deg as shown in Figure 1. Fuel was injected on the rough flat window surface at various ambient conditions, injection conditions and distance between the injector tip and window, using the same optical setup.

Numerical Investigation

Simulation of the spray behavior and impingement was carried out using the multi-dimensional CFD code CONVERGE [24]. In the present spray simulation study, the Reynolds Averaged Navier-Stokes (RNG) k-epsilon model was used for turbulence transport. Variations in the drop shape, the drop drag coefficients were obtained by the dynamic drag model. The collision and coalescence of droplets was simulated by the No Time Counter (NTC) method. The standard vaporization model was used to calculate the time rate of change of droplet radius due to ethanol vaporization.

The Kelvin-Helmholtz/Rayleigh-Taylor (KH-RT) breakup model was used to predict the spray behavior of MHN injector. The KH model simulated the primary aerodynamic instabilities breakup and the RT model calculated the secondary breakup due to decelerative instabilities. For KH-RT breakup model, the breakup length was written as

$$L_b = C_{bl}\sqrt{\frac{\rho_l}{\rho_g}}d_0 \tag{3}$$

where ρ_l and ρ_g are the density of the fuel liquid and the ambient gas, d_0 is the diameter of the orifice, C_{bl} is the breakup length constant, which was set to 5. The KH breakup time constant was determined to be 12 in this study after comparison with the experimental results. Only KH instabilities are responsible for drop breakup inside of the breakup length, while both KH and RT mechanisms are activated beyond the breakup length.

The interaction of liquid drips and solid surfaces is modeled using a wall film model, which is a hybrid model that assumes individual particle-based quantities and film-based quantities [25]. The liquid film transport is modeled by the film momentum equation [26]. The drop Weber number is defined as

$$We = \frac{\rho_l V_n^2 d}{\sigma} \tag{4}$$

where ρ_l is the liquid density, V_n is the drop velocity component normal to the surface, d is the drop diameter, and σ is the liquid surface tension. In this study, if the drop Weber number is less than 5, the drop is assumed to rebound. The criterion for splash [26] is given by

$$E^2 = \frac{We}{\min\left(\frac{h}{d},1\right)+\frac{\delta}{d}} > E^2_{criterion} \tag{5}$$

Where h is the local film thickness and δ is the boundary layer thickness calculated from the drop diameter and Reynolds number. $E_{criterion}$ is set to 57.45 based on the experimental work in [27].

The computational grid and spray targeting in this study are shown in Figure 5. The computational domain is a cylinder of Φ120mm × 40mm. The number of cells was about 150,000. The mesh size was: 2mm for the central region, 0.5mm for the injector nozzle area, and 1mm for the impinging boundary. Adaptive Mesh Refinement (AMR) was used in CONVERGE to automatically enhance the mesh resolution based upon gradients in field variables, such as velocity, temperature and species.

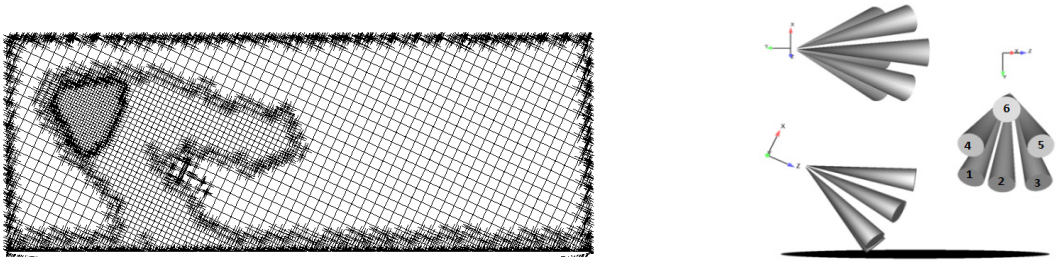

Figure 5 Computational grid (left) and spray targeting (right) for the MHN injector**.**

Results

Refractive Index Matching method was performed to measure the fuel film thickness, spatial distribution and adhered puddle mass for a side-mounted multi-hole injector under different operating conditions.

The processing of RIM experiment images was shown in Figure 6. First, the averaged reference image was subtracted from the wetting images to calculate the reduction in scattered light ΔI. This was then converted to a binary image that was used to obtain the instantaneous area of deposit film. The threshold that converts the intensity image into the binary image was calculated by Otsu's method, which minimizes the intraclass variance of the black and white pixels. To eliminate the noise on the background image, time and space filtering were carried out to improve the image quality. For the time filter, a fixed-point filter is used to average a sequence of images with window size of 10. For the space filter, a mean filter is adapted to 4x4 blocks. Figure 6 (d) and (e) show the filled contour of images that applied the time filter and space filters, respectively. Color coded image is used to accentuate the intensity, with the red region representing a high intensity, and blue region, low intensity.

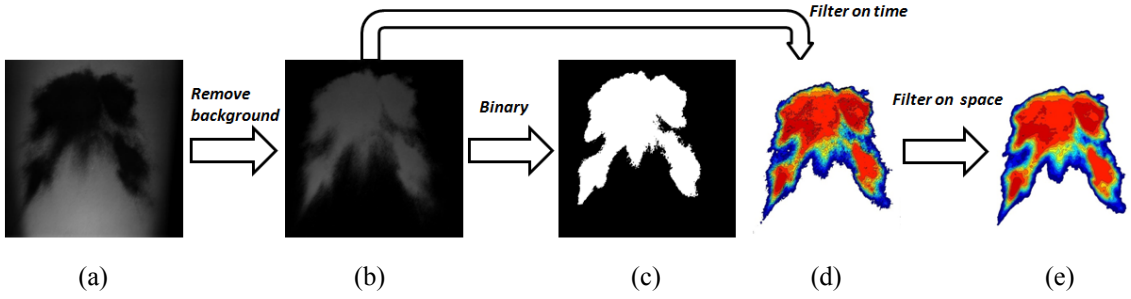

Figure 6 Image processing of the RIM images, (a) Raw image, (b) Background removed image, (c) Binary image, (d) Time filtered image, and (e) Time and space filtered image

Evolution of the fuel film thickness, mass and spatial distribution after fuel deposit on the window is presented in Figure 5 for cases 1, 2, 3 and 4 to illustrate the effect of injection pressure (35bar and 140bar), injection duration (1.41ms and 2.83ms) and distance between the injector tip and window (30mm and 40mm). For injection emerging from the multi-hole GDI injector, mean film thickness results from spray plumes were investigated. The mean film thickness is an instantaneous average over the entire area of deposit film. As the spray targeting scheme shown in Figure 5, three lower spray plumes first impinge the window and then the two middle plumes (4^{th} and 5^{th}) land later. The last plume (6^{th}) does not meet the window for all cases in this study. Therefore, up to five wetted spray footprints could be measured.

The dynamic evaporation can be found from the film thickness spatial distribution in Figure 7, thinner film (blue) evaporates fast and thicker film (red) has slower evaporation. The wetted areas of cases 2 and 4 are much larger than the areas of cases 1 and 3 respectively due to the high injection pressure. The camera speed is 1000fps for RIM test, which is not fast enough to record the process of spray impinging, so that the curves of averaged film thickness and mass in Figure 8 could be roughly extended to initial deposit time though the line slope, which presents the rate of evaporation. Also, the gently sloping curves of cases 1 and 3 are result of saturation of the rough surface of the window. Therefore, the maximum film thickness of the RIM measurement in this study is underestimated. For the high injection pressure cases 2 and 4, the film evaporates much faster after deposition on window, compared with cases with 35bar injection pressure. The reason of the larger film area and faster evaporation for the high injection pressure cases is that the velocity at which droplet impacts is higher and the atomization of spray is better. For case 3 and 4, the distance between injector tip and window is 40mm, as shown in Figure 7, the film thickness and deposit area of the 4^{th} and 5^{th} spray plumes were much thinner and smaller compared with 30mm distance cases.

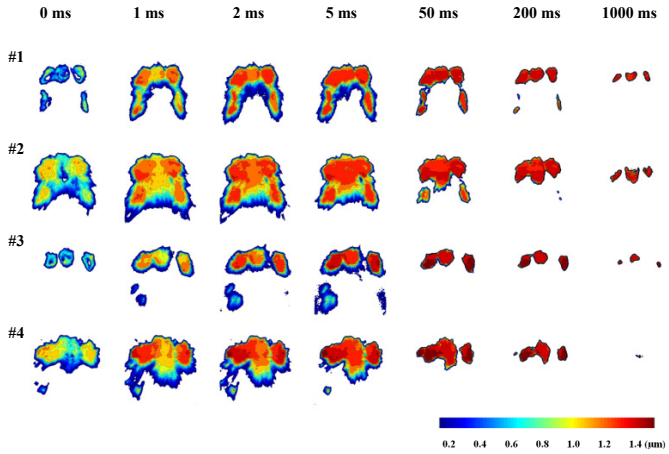

Figure 7 Evolution of fuel film thickness and spatial distribution (Case#1~4) after fuel droplet deposit on window

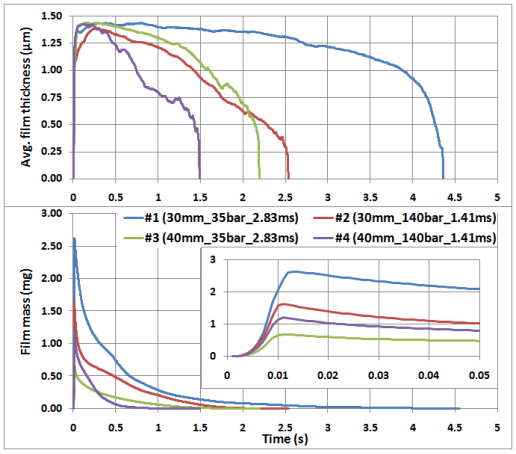

Figure 8 Averaged film thickness and film mass after fuel droplet deposit on window (Case#1~4)

The film mass in Figure 8 was calculated from the averaged film thickness and the corresponding film deposit area. Case 1 has the longest evaporation time due to its low injection pressure and long injection duration. The maximum film mass of case 1 is around 3 mg at time zero (by extrapolation) and takes over 4 seconds to completely evaporate. Case 2 has a higher injection pressure than case 1, but both cases have the same injection mass (24.5mg), therefore case 2 has a shorter injection duration. The higher injection pressure resulted in lower film thickness and mass, and consequently faster film evaporation. For cases 3 and 4, which have significantly different wetted footprints due to greater impact distance, the effects of injection pressure on film thickness and mass are similar, at least in the beginning.

The effects of ambient pressure (1bar and 2bar), ambient temperature (50°C, 75°C, and 100°C), and fuel temperature (40°C, 55°C, and 70°C) were investigated and shown in Figure 9 and 10. Ambient temperature, which includes the impinging place, and fuel temperature were increased together to represent the warm up of an engine. For cases with 1bar air pressure (5, 7 and 9), the film thickness decreases faster with increasing temperature as shown in Figure10. For the cases of 2bar air pressure (6, 8, and 10), the maximum film thickness are higher than the ones with 1bar ambient pressure, at corresponding temperatures. The rate of evaporation is much slower for the 2bar air pressure cases, especially at low temperature. Comparing the results in Figure 9 and 10, it is obvious that the temperature has the most dominant effects on fuel film thickness and mass. Ambient pressure has a secondary role on the film mass, but has a stronger effect on the rate of film mass evaporation.

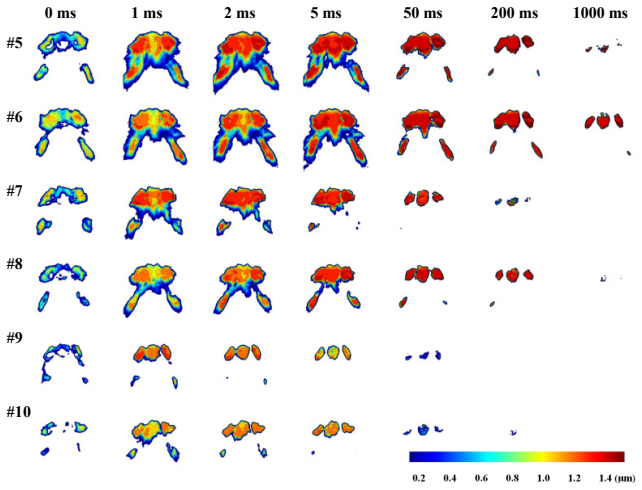

Figure 9 Evolution of fuel film thickness and spatial distribution (Case#5~10) after fuel droplet deposit on window

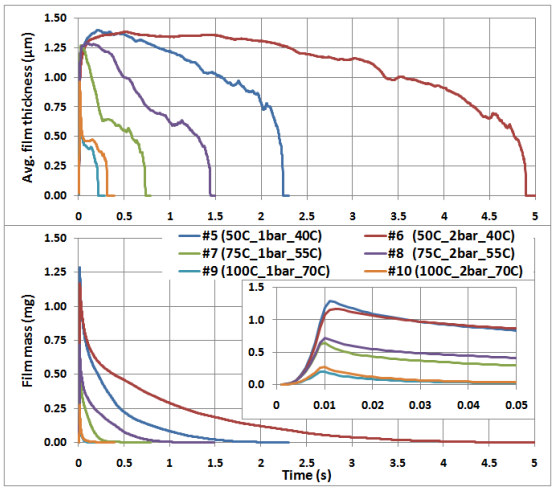

Figure 10 Averaged film thickness and film mass after fuel droplet deposit on window (Case#5~10)

In this study, numerical simulation of the multi-hole spray injection was carried out using multi-dimensional CONVERGE CFD codes. In each case, around 60,000 parcels of fuel spray were tracked for sufficiently pre-

cise statistical resolution. In order to obtain a better agreement of the spray impingement and wall fuel film of the multi-hole injector, back-lighting was chosen to illuminate the free spray transport process first and then the spray impinging process. Figure 11 shows the comparison of free spray development for case 5 and 6. The simulated spray is also shown in this figure and good agreement between back-lighting visualization and calculations is obtained with respect to spray cone angle, tip penetration and general shapes. The size of background grids is 5mm × 5mm.

Experimental evolution of the impinging spray was compared with simulation results in Figure 12. Fuel droplets deposited on the window around 0.6ms after the start of injection. For the multi-hole injector in this study, one spray plume will not reach the window surface as shown in the figure. The spray cone angle and tip penetration of the experimental spray were compared with computational results and also show very good agreement.

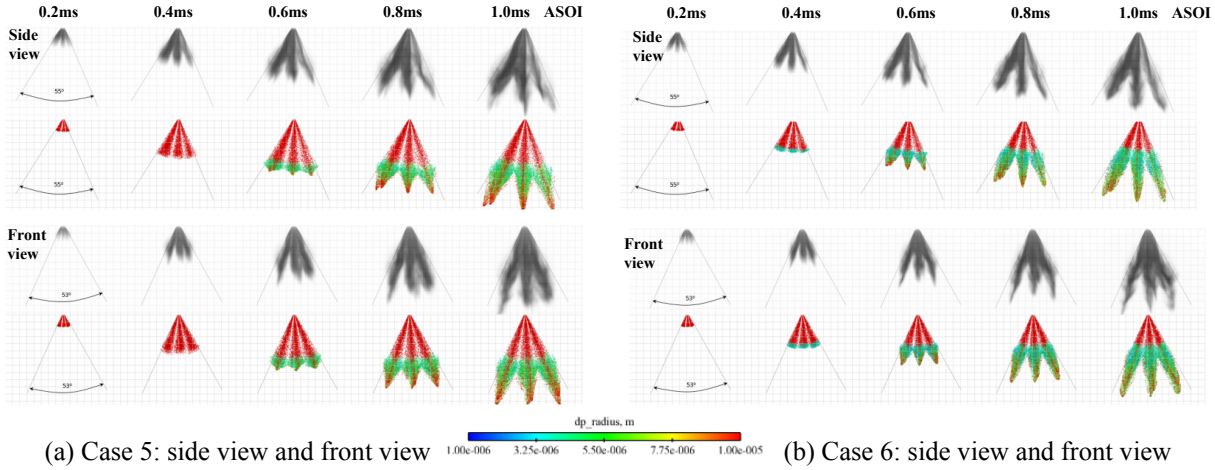

(a) Case 5: side view and front view (b) Case 6: side view and front view

Figure 11 Comparison of experimental free spray evolution and CFD-simulation (3D parcel representation)

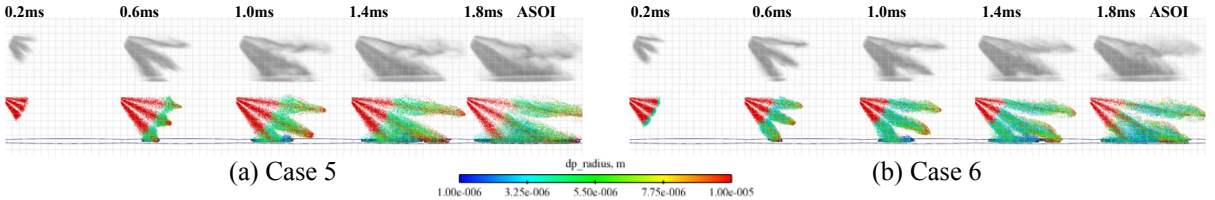

(a) Case 5 (b) Case 6

Figure 12 Comparison of experimental impinging spray and CFD-simulation (3D parcel representation)

Comparison of the experimental liquid film measurement and simulation is shown in Figure 13 and 14. Injection mass in this work keeps 24.5mg. The spray deposit area and shape have reasonable agreement as shown in Figure 13. The simulation result of film spatial distribution shows higher film thickness around the center of each puddle. The computational value of maximum film thickness is about 1.2µm, which is very close to the experimental result of 1.4 µm. The numerical grid size of the impinging surface is 1mm, and the experiment image processing is based on 1 pixel (0.15mm). This may be the main reason that why the simulation contour profile of film distribution is not as smooth as the experimental contour plot. Although the evolution of film mass evaporation shows similar trends, the calculated maximum film mass is consistently higher than the experimental values. As shown in Figure 14, the simulated film mass is higher than the corresponding RIM experimental results. The reason for this discrepancy may have to do with the surface roughness of the ground glass diffuser and/or the modeling of spray impingement processes, and will be the subject of further investigation.

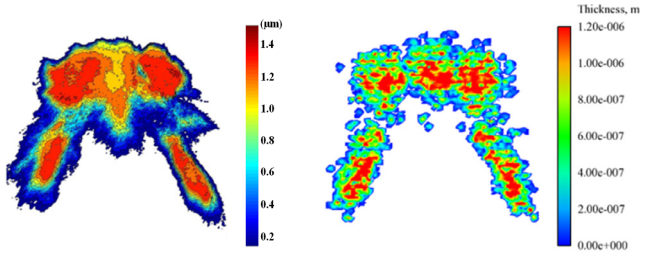

Figure 13 Comparison of experimental fuel film thickness and spatial distribution (left) and CFD-simulation (right), 2.6ms after start of injection (Case#6)

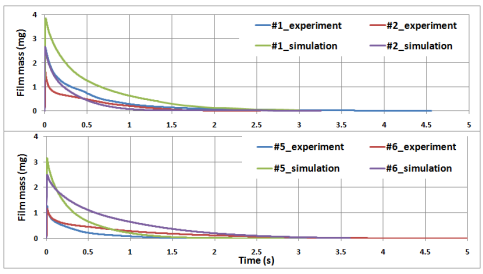

Figure 14 Comparison of experimental fuel film mass and CFD-simulation (Case#1, 2, 5 and 6)

Summary and Conclusions

In this work experimental and computational investigations were carried out for the spray wall interactions of a side-mounted DI gasoline multi-hole injector. The Refractive Index Matching technique was used to characterize and measure the fuel film thickness of wetted footprints in a conditioned pressure chamber. The results show that the effect of ambient temperature on fuel film thickness was very significant, and the film evaporation rate was also strongly affected by the ambient pressure especially at lower temperature. The deposit area and shape of each spray plume was affected by the injection pressure and the distance between injector tip and window. Higher pressure at the same fuel amount tends to reduce film thickness. CFD simulation was also conducted, validated first with spray visualization on the free spray transport and then compared with the RIM test results. The numerical investigation of spray behavior and film characteristics agrees in general with the experimental observations in terms of overall spray shape, tip penetration and wall impingement pattern, and the maximum fuel film thickness. However, the predicted fuel mass is greater than the RIM results possibly due to the surface roughness and the modeling of spray impingement.

Acknowledgements

This work is partially supported by Ford Motor Company. The use of Converge code supplied by Convergent Science is also greatly appreciated.

References

[1] Kalantari D. and Tropea C., Int. J. Multiphase Flow, 2007, 33, p. 525-544.
[2] Moreira, A.L.N., Moita, A.S., and Panao, M.R., Prog. Energy Combust. Sci., 2010, 36, 544-580.
[3] Matsumoto, A., Zheng, Y., Xie, X, Lai, M.-C., Moore, W., Yen, D., Hopkins, E., Foster, M., Confer, K., SAE Int. J. Engines, 3(1), 2010:402-425, (2010).
[4] Hung D., Zhu, G., Winkelman, J., Stuecken, T. et al., SAE Technical Paper 2007-01-1411, (2007).
[5] Yoo, J., Zhao, F.-Q., Lai, M.-C., and Lee, K.-S., SAE Technical Paper 982702, (1998).
[6] Park, J., Xie, X., Im, K.-S., Kim, H., Lai, M.-C., Yang, J., Han, Z., and Anderson, R., SAE Technical Paper 1999-01-3662, (1999).
[7] Stanglmaier, R.H., Li, J., and Matthews, R.D., SAE Technical Paper 1999-01-0502, (1999).
[8] Park, J., Xie, X., Im, K.-S., Kim, H., Lai, M.-C., J. Fuels & Lubricants, SAE Transc. 110(4), pp. 1517-1536, (2001).
[9] Park, J., Im, K.-S., Kim, H., and Lai, M.-C., Int. J. Automotive Technology, 5(4), pp. 221-238, (2004).
[10] Mathews, W.S., Lee, C.F., Peters, J.E., Atomization and Sprays 13:223-242 (2003).
[11] Borthwick, R.P., Farrell, P.V., F, SAE Technical Paper 2002-01-0496, (2002).
[12] Fan, Q., Li, L., Hu, Z., and Deng, J., SAE Technical Paper 2011-01-1222, (2011).
[13] Zhao, F., M.-C. Lai, and D.L. Harrington, Progress in Energy and Combustion Science, 1999. 25: p. 437-562.
[14] Drake, M., Fansler, D. and Rosalik, M.E., 15th Annual Conference on Liquid Atomization and Spray Systems, Madison,WI, May 2002.
[15] Drake, M., Fansler, D. Solomon, A.S., and Rosalik, M.E., SAE Technical Paper 2003-01-0547, (2003).
[16] Yang, B., Ghandhi, J., SAE Technical Paper 2010-01-0485, (2010).
[17] Maligne, D., Bruneaux, G., SAE Technical Paper 2011-01-1215, (2011).
[18] Lindgren, R., and Denbratt, I., SAE Technical Paper 2004-01-1951, (2004).
[19] Park, S.W., Lee, C.S., Atomization and Sprays 13:517-534 (2003).
[20] Befrui, B., Corbinelli, G., D'Onofrio M., Varble D., SAE Technical Paper 2011-01-1211, (2011).
[21] Montorsi, L., Magnusson, A., and Andersson, S., SAE Technical Paper 2007-01-0486, (2007).
[22] Montanaro, A., Malaguti, S., Alfuso, S., SAE Technical Paper 2012-01-1266, (2012).
[23] Karlsson, R. B. and Heywood, J. B., SAE Technical Paper 2001-01-2022, (2001).
[24] Richards, K.J., Senecal P.K., and Pomraning E. CONVERGE™ (Version 1.3). Middleton, WI: Convergent Science, Inc (2008).
[25] Schmidt, D. P., Nouar, I., Senecal, P. K., Hoffman, J., Rutland, C. J., Martin, J., and Reitz, R. D., SAE Technical Paper 1999-01-0496, (1999).
[26] O'Rourke, P. J. and Amsden, A. A., SAE Technical Paper 2000-01-0271, (2000).
[27] Mundo, Chr., Sommerfeld, M. and Tropea, C., Int. J. Multiphase Flow, Vol. 21, p. 151 (1995).